Int. J. Electrochem. Sci., 14 **(2019)** 4933 – 4945, doi: 10.20964/2019.06.45

International Journal of
ELECTROCHEMICAL
SCIENCE
www.electrochemsci.org

Short Communication

All-solid-state Ca^{2+} Ion-selective Electrode with Black Phosphorus and Reduced Graphene Oxide as the Mediator Layer

Qingliang Yang[1], *Miao Zhang* [1,2*], *Chen Ming* [1], *Gang Liu* [1,2],*Maohua Wang* [1,2]

[1] Key Laboratory on Modern Precision Agriculture System Integration Research of Ministry of Education, China Agricultural University, Beijing, China 100083.
[2] Key Lab of Agricultural Information Acquisition Technology, China Agricultural University, Beijing, China 100083.
[*]E-mail: zhangmiao@cau.edu.cn

Received: 29 January 2019 / *Accepted:* 23 March 2019 / *Published:* 10 May 2019

An all-solid-state Ca^{2+} ion-selective electrode (Ca^{2+}-ISE), employing a composite mediator layer of reduced graphene oxide (RGO)-coated black phosphorus (BP), was developed and analyzed. The morphological characteristics of the prepared Ca^{2+}-ISE were compared with those of other Ca^{2+}-ISEs with solid-contact monolayers of RGO or BP. The potentiometric performance of the designed ISE was systematically verified. An ideal Nernstian response was observed with a stable linear range from 1.0×10^{-6}-1.0×10^{-1} M, a response slope of 28.3 mV/decade, and a limit of detection of 7.2×10^{-6} M. Due to the outstanding hydrophobic performance of the RGO-coated mediator film, the potential drift of the Ca^{2+}-ISE decreased to 0.01 mV s^{-1}. In addition, the ISE demonstrated good stability with a negligible potential variation of less than 2.86 μV s^{-1} when exposed to a variety of interferences, such as ambient light and gases. The sensitivity was maintained at a satisfactory level after continuous use over 10 days. Real lettuce nutrient solutions were applied to validate the feasible application of this ISE. Promising capabilities were found with detection recovery rates ranging from 87% to 112%.

Keywords: Calcium; All-solid-state ion-selective electrode; Black phosphorus; Reduced graphene oxide; Composite mediator layer.

1. INTRODUCTION

In recent decades, calcium ion-selective electrodes (Ca^{2+}-ISEs) have been reported with applications in clinical diagnosis, biological detection, and crop management [1-5]. Working as a chemical species inside of a liquid polymeric membrane, calcium ionophores selectively bind to Ca^{2+} and shield their charges from the surrounding environment. The calcium salt of dodecylphosphonic

acid was synthesized as a first-generation Ca^{2+} ionophore due to the charge attraction between its two anion phosphate group and a calcium cation [6]. ETH 1001 combined with $KB(ClPh)_4$ was then used as a Ca^{2+} ionophore because of its enhanced electrostatic interactions and electric conductivity [7]. ETH 129 was reported to have an approximately 20-fold greater ion transport efficiency than that of ETH 1001 due to its structure of nine diamide oxygen atoms, which could form a cavity of the ideal size for calcium ions [8-9]. Based on the mechanism for charged analyte-gated permeability changes, ETH5234 has recently been utilized as an immobilizing ionophore for ion-channel mimetic sensors (ICSs) due to being more lipophilic than ETH 129 [10].

By eliminating the hollow-structure and inner filling solution, an all-solid-state calcium ion-selective electrode (Ca^{2+} SC-ISE) was shown to demonstrate advantages in terms of its robustness and cost-effective fabrication and maintenance [11, 12]. The water layer that formed between ISM and the conductive electrode during continuous detection largely degraded the stability and reproducibility of the Ca^{2+} SC-ISEs [13]. To solve this problem, conductive polymers, such as polypyrrole (PPy) and poly(3,4-ethylene-dioxythiophene) (PEDOT), and nanomaterials, such as carbon nanotubes, gold nanoclusters, and MoS_2 nanoparticles, have been attempted as mediator layers [14]. Ca^{2+} SC-ISEs with mediator layers showed improved ion-to-electron transfer. Recently, graphene and its composites have demonstrated unique electrical conductivities and charge carrier mobilities, which have made them popular candidates for the synthesis of mediator layers [15, 16]. Black phosphorus (BP), a two-dimensional mediator material, has received worldwide attention due to its potential low cost and similar physicochemical properties as those of graphene, and BP has been applied as the mediator layer of SC-ISEs for sensing air humidity, NH_3/NO_2, and heavy metal ions [17]. In addition, BP has also been employed for the biochemical sensing of myoglobin, proteins, and immunoglobulin [18]. However, BP faces a major application bottleneck due to its hydrophilicity caused by being gradually oxidized in ambient environments [19, 20]. Passive surface protection films, such as AlO_x, hexagonal boron nitride crystals, and SiO_2, have been coated on top of BP to serve as antioxidation films [20-22]. However, the performance of interface-passivated BP has barely been satisfactory. Reduced graphene oxide-coated BP (BP/RGO) has demonstrated long-term stability (ca. 100 h) with double and triple layer passivation [23]. However, the chemical vapor deposition (CVD) coating method is complex and time consuming [24]. A recent study reported that the oxidative degradation of BP was largely inert under water [25]. Inspired by this result, BP/RGO might be feasibly fabricated through an electrochemical reduction process conducted in solution.

Thus, a novel solid-state calcium ISE with a composite mediator layer of BP/RGO was designed and tested for stability enhancement and water-layer elimination. The RGO-coated BP was innovatively synthesized through an electrochemical reduction in solution. The electrochemical performance of the designed Ca^{2+}-ISE was systematically tested. Furthermore, its feasibility for the detection of hydroponic nutrients was verified.

2. MATERIALS AND METHODS

2.1 Reagents and apparatus

Calcium ionophore IV (*N*,*N*-dicyclohexyl-*N*′,*N*′-dioctadecyl-diglycolic diamide, ETH 5234, Selectophore™), bis(2-ethylhexyl) sebacate (DOS, Selectophore™), sodium tetrakis[3,5-bis(trifluoromethyl)phenyl]borate (NaTFPB, Selectophore™), and tetrahydrofuran (THF) were purchased from Sigma-Aldrich (China). Black phosphorus powder (99.9%) and a graphene oxide (GO) dispersion (2 mg/mL) were purchased from Nanjing XFNANO Materials Tech. (Nanjing, China). All other chemicals mentioned in this paper were purchased from Tianjin Chemical Reagent (China) at analytical reagent grade. Deionized water (18.25 MΩ) was used to prepare solutions.

The reference electrode (R0303, Ag/AgCl in 3.5 M KCl), counter electrode (Pt017, platinum wire, Φ1.0 mm × 37 mm), and working electrodes (GC150, glass carbon electrode (GCE, Φ5.0 mm × 80 mm) were ordered from IDA, China. Field-emission scanning electron microscopy (FESEM, SU8020, Hitachi, Japan) was used to characterize the morphologies of the ISEs. X-ray powder diffraction (XRD) analysis was conducted using an XPert-Pro (PANalytical, Netherlands). A CHI660D electrochemical workstation (CH Instruments Inc., USA) was employed for all potential performance testing.

2.2 Electrode preparation and modification

The GCEs were polished with 0.05 μm alumina slurries, ultrasonicated with anhydrous ethanol, and rinsed with deionized water for further use. A 2 mg/mL BP dispersion was achieved by sonicating 10 mg BP in 5 mL anhydrous ethanol for 3 h [26]. A volume of 5 μL of the BP dispersion was drop-casted onto a GCE and then blown dry with N_2. The drop-casting process was repeated 5 times. A uniform BP mediator layer with a thickness of 200 μm was obtained. Reduced graphene oxide was deposited through electrochemical reduction. A controlled volume of 8 μL of the GO dispersion was drop-cast onto the BP/GCE. The electrochemical reduction was carried out in 0.1 M PBS (pH 4.0) solution. A constant potential of -1.4 V was applied against the GCE and RE for 15 min. The analyte solution was purged with N_2 10 min prior to the electrochemical reaction. A visible dark layer corresponding to the RGO film was deposited onto the surface of the BP/GCE. A composite mediator layer of RGO/BP was synthesized. The GC/BP/RGO electrode was rinsed with deionized water and then blown dry with N_2. Electrodes with single-mediator films of BP or RGO were fabricated under similar conditions for further comparison.

According to previous reports [27], Ca^{2+} ion selective membranes (Ca^{2+}-ISMs) have been synthesized with ETH 5324 (1.0 wt%), NaTFPB (0.5 wt%), PVC (33.0 wt%), and DOS (65.5 wt%). A total of 500 mg of the membrane components were dissolved in 5 mL of tetrahydrofuran (THF). After sonicating for 10 min, the mixed ISM components were poured into a culture dish (Φ60.0 mm). Then, a transparent ISM membrane was obtained after evaporation of the THF in a fume hood for 36 h. ISMs with a diameter of 5 mm were cut from the mold with a round punch module (63656-1EA,

Selectophore™, Sigma-Aldrich, China). Then, the above membrane disks were pasted onto the surface of a GC/BP/RGO electrode with a volume of 4 µL of THF. The prepared electrode was labelled GC/BP/RGO Ca^{2+}-ISE. The fabricated Ca^{2+}-ISEs were air-dried in a fume hood for 24 h at room temperature. GC/BP and GC/RGO Ca^{2+}-ISEs were fabricated by gluing the Ca^{2+}-ISM disks to the surface of the single mediator layers of BP or RGO by the abovementioned procedures for further comparisons. All prepared Ca^{2+}-ISEs were conditioned in a 10^{-3} M $CaCl_2$ solution overnight before testing. A schematic diagram of the Ca^{2+}-ISEs with different mediator layers is shown in Fig. 1.

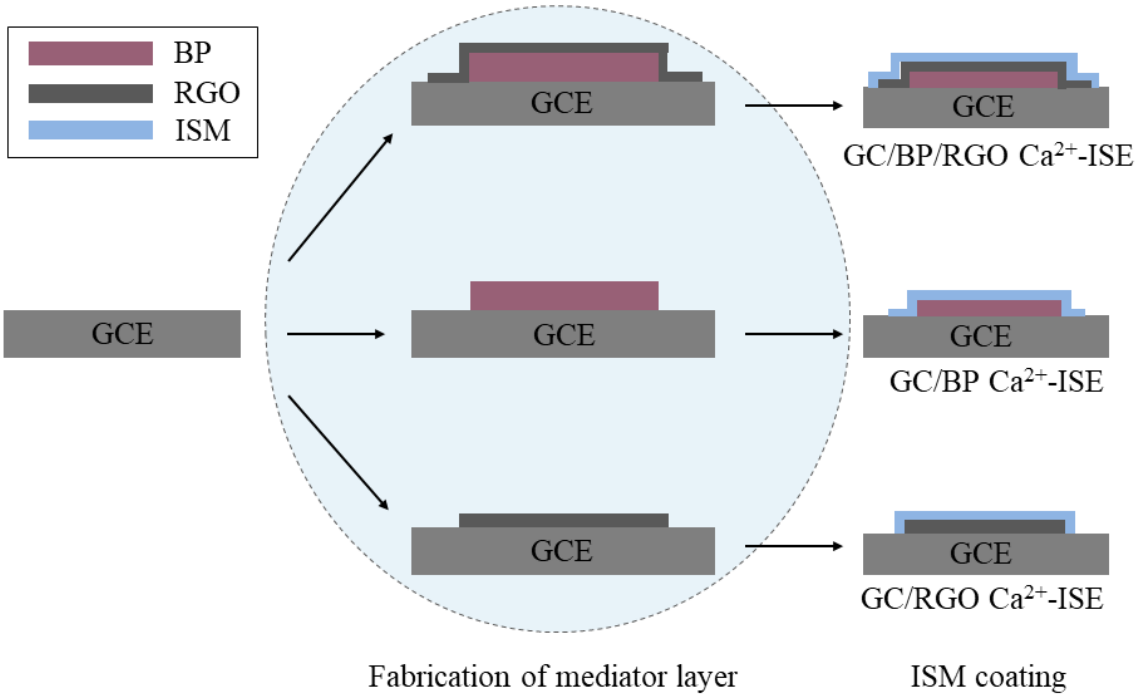

Figure 1. Schematic illustration of the structure of the GC/BP/RGO, GC/BP and GC/RGO Ca^{2+}-ISEs.

2.3 Morphological characteristics of the mediator film

The morphological characteristics of RGO/BP, BP, and RGO were compared through FESEM at two different image magnifications, as shown in Fig. 2(a-f). BP flakes were formed through dispersion and exfoliation in anhydrous ethanol. The synthesized BP was found to have a morphology of randomly oriented thin BP flakes after evaporation of the anhydrous ethanol. As seen in Fig. 2(c), a BP flake with an oval shape and a large diameter of 45 µm was observed, which was consistent with the results of previous studies [28, 29]. RGO/BP demonstrated similar morphological characteristics, with an oval-shaped border in the FESEM image as shown in Fig. 2(a). The detailed textural features were related to the top material of the mediator layer. The surface of the plain BP flake was smooth with minimal morphologic changes, as shown in Fig. 2(d). In contrast, RGO/BP exhibited visible floc- and stripe-like structures in Fig. 2(a). The detailed floc and stripe shapes on the surface are also shown in Fig. 2(e). Furthermore, in Fig. 2(b) and 2(f), the RGO/BP composite film clearly revealed a similar well-organized structure as the individual RGO. The uniform surface textural features agreed well with the reported morphological characteristics of RGO [30-32]. Evidently, the BP mediator layer was

successfully coated with reduced graphene oxide. RGO acted as an antioxidant layer for BP according to its designed purpose.

The heterostructure formed from RGO/BP layers was further confirmed by XRD, as shown in Fig. 3. The three peaks with 2θ values of 16.9°, 34.2° and 52.3° matched well with the peaks of the standard BP pattern for the (020), (040) and (060) planes (JCPDS 73-1358) [33]. The BP layer was maintained in the non-oxidized state after the electrochemical reduction of RGO. At the same time, the characteristic peak of GO, with a 2θ of 11°, did not appear in the diffraction pattern [34]. The RGO layer was successfully synthesized on top of the BP.

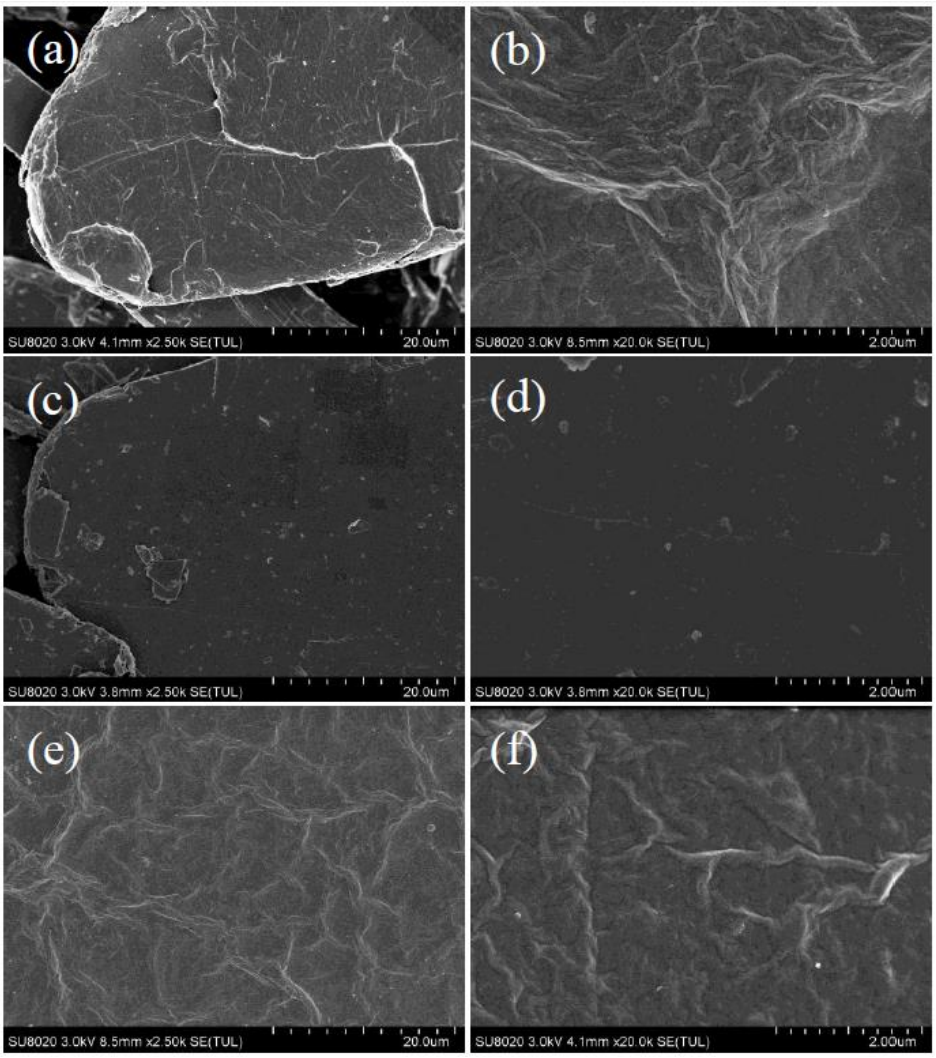

Figure 2. Basic characterization of BP, RGO and BP/RGO. (a) FESEM image of layered BP/RGO on the surface of an electrode at 20 μm. (b) FESEM image of layered BP/RGO on the surface of an electrode at 2 μm. (c) FESEM image of BP flakes drop-cast on the surface of an electrode at 20 μm. (d) FESEM image of BP flakes drop-cast on the surface of an electrode at 2 μm. (e) FESEM image of RGO deposited on the surface of an electrode via the electrochemical reduction method at 20 μm. (f) FESEM image of RGO deposited on the surface of an electrode via the electrochemical reduction method at 2 μm.

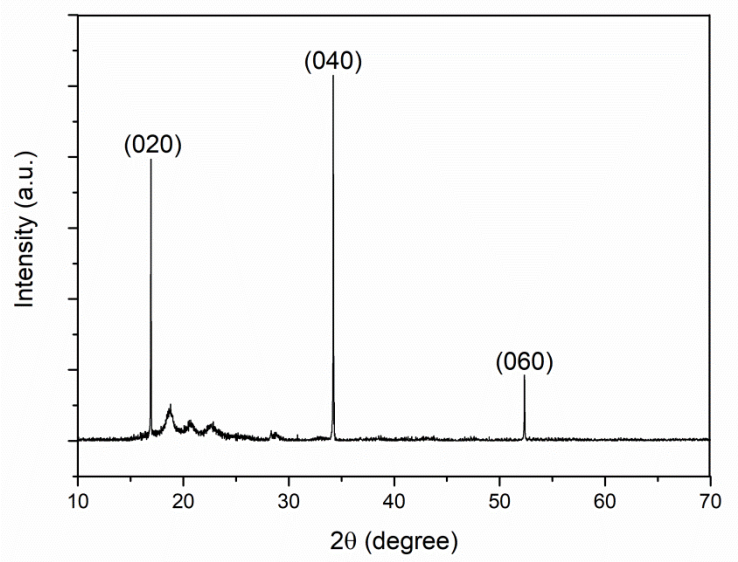

Figure 3. XRD pattern of the BP/RGO mediator film

2.4 Experimental Design

Chronopotentiometric performances were compared among the Ca^{2+}-ISEs prepared with different mediator layers. A constant current of +1 nA was first applied to the Ca^{2+}-ISEs, while the potential between the Ca^{2+}-ISEs and the reference electrode was measured in a 10^{-3} M $CaCl_2$ solution. Then, a reverse current of the same magnitude was subsequently applied for another 60 s [35]. The current difference through the all-solid-state Ca^{2+}-ISE was proportional to the measured potential change. By introducing a constant of proportionality, the resistance (R) of the electrode could be calculated by Ohm's law. The value of the resistance was used to evaluate the conductivity differences of the tested mediator films.

Stability tests were examined based on the results of the potential drifts caused by the water layer [13]. Experiments were carried out continuously for 10 h with alternate determinations performed in solutions with primary and interference ions. The Ca^{2+}-ISEs were tested in a 10^{-1} M $CaCl_2$ solution for the first 2 h. Then, detection measurements were conducted in a 10^{-1} M $MgCl_2$ solution for another 2 h. Finally, an extra 6 h of detection was performed in a 10^{-1} M $CaCl_2$ solution. The stability was evaluated based on the unit-time potential differences between the collected results of the first and the last tests in the 10^{-1} M $CaCl_2$ solution. The intermediate stability was also determined from the unit-time potential drift during the last 6 h. Smaller variations represented better performance.

The electrochemical performance of the Ca^{2+}-ISEs were measured in $CaCl_2$ solutions with 10-fold serial dilutions ranging from 1.0×10^{-1} to 1.0×10^{-6} M. ISE readings was recorded at an interval of 10 times/s for 80 s in each solution. The sensitivity was characterized by the slope of the calibration curve and the limit of detection (LOD). The response rate of the ISE was quantified as a factor of the response time, which was defined as the elapsed time between the moment of contact with an aqueous sample and the first instance of achieving 95% of the equilibrium potential [36].

According to a previous report [30], ambient air, especially CO_2, and light, may disturb the performance of an ISE. Ca^{2+}-ISEs with the RGO/BP composite mediator layer were examined under numerous independent environmental conditions, including room light, UV light, infrared light, N_2, O_2, and CO_2. The tests were conducted in a 10^{-1} M $CaCl_2$ solution.

The prepared GC/BP/RGO ISEs were evaluated for continuous Ca^{2+} detection in hydroponic lettuce cultivation. Green oak leaf lettuce (Lactuca sativa, Futong, Beijing, China) was grown at the experimental station of the China Agricultural University, Beijing, China. The hydroponic nutrient solution was prepared according to the recipe reported by Cornell University [37]. Three hydroponic solution samples were collected on the 2nd, 6th and 13th day of lettuce cultivation. A self-designed detection platform was employed in this research [38]. The recovery rate was used to evaluate the accuracy and repeatability of the ISEs through a solution addition method. The recovery rates was calculated according to eq. (1).

$$F_{\mathrm{RR}} = \frac{(c_2 - c_1) \times V_1}{c_0 \times V_0} \times 100\% \quad (1)$$

where F_{RR} is the recovery rate; c_0, c_1 and c_2 represent the molar Ca^{2+} concentrations of the artificial standard solution added to the principle solution, the original hydroponic sample, and the sample solution after solution addition, respectively, M; V_0 and V_1 represent the reagent volumes of the artificial standard solution and the sample, respectively. These volumes were chosen to be 50 μL and 50 mL for these tests.

3. RESULTS AND DISCUSSION

3.1 Chronopotentiometric performance

Three types of Ca^{2+}-ISEs with different mediator films, including GC/BP/RGO, GC/BP and GC/RGO Ca^{2+}-ISEs, were tested through a constant-current chronopotentiometry method. Their potentiometric responses are shown in Fig. 4. A distinct potential change was observed at 60 s when the applied current was reversed in polarity. The electrode resistances were calculated by dividing the potential changes by the applied current differences. Thus, the resistances of GC/BP/RGO, GC/BP and GC/RGO were found to be 0.50, 6.22 and 3.03×10^{-6} Ω, respectively. The ISE with the composite mediator layer of RGO-coated BP possessed the best conductivity. The conductivity of the GC/BP/RGO Ca^{2+}-ISE was similar to the result of a leading peer-reviewed study on a polyaniline-coated graphene (PANI/GR) Ca^{2+}-ISE, which had a resistance value of 5.0×10^{-7} Ω [39].

The potential drift was estimated from the potential variation ratio of $\Delta E/\Delta t$ over the testing duration of 61-120 s [35]. The values of $\Delta E/\Delta t$ for the GC/BP, GC/RGO and GC/BP/RGO Ca^{2+}-ISEs demonstrated a decreasing trend of 0.136, 0.016, and 0.01 mV s^{-1}, respectively. The prepared GC/BP/RGO Ca^{2+}-ISE declined to 7.4% and 62.5% of the potential drift amplitudes observed for the GC/BP and GC/RGO Ca^{2+}-ISEs, respectively. Most of the previously reported all-solid-state Ca^{2+}-ISEs have exhibited a similar stability performance as the GC/BP Ca^{2+}-ISE with $\Delta E/\Delta t$ values ranging from 0.1-1.0 mV s^{-1} [39, 40]. The GC/BP/RGO Ca^{2+}-ISE demonstrated an overwhelmingly consistent

stability, which was mainly related to the heterostructure of its composite mediator layer and the complementary properties of the two constituents [41, 42].

3.2 Stability performance

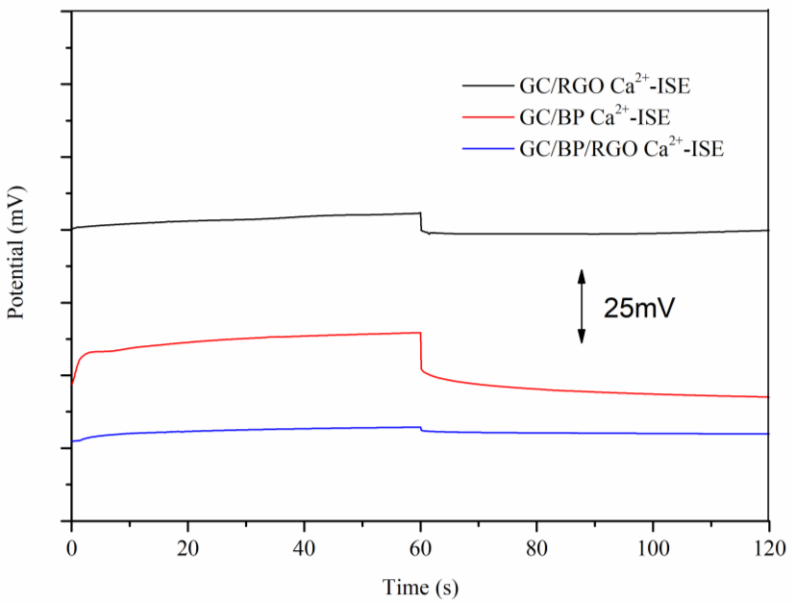

Figure 4. Chronopotentiograms of GC/RGO Ca^{2+}-ISE (black), GC/BP Ca^{2+}-ISE (red), and GC/BP/RGO Ca^{2+}-ISE (blue) recorded in a 10^{-3} M $CaCl_2$ solution. The applied currents were set at ±1 nA for 60 s, sequentially.

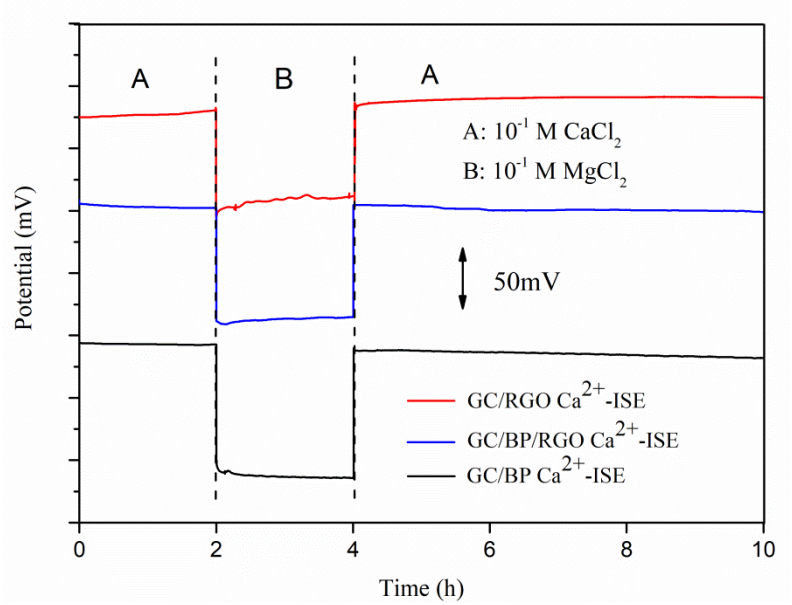

Figure 5. Stability performance of GC/RGO Ca^{2+}-ISE (red), GC/BP/RGO Ca^{2+}-ISE (blue), and GC/BP Ca^{2+}-ISE (black). The measurements were switched between a 10^{-1} M $CaCl_2$ solution (A) and a 10^{-1} M $MgCl_2$ solution (B).

Hydrophobic solid mediator films have been shown to decrease the formation of a water layer [39, 43]. Potentiometric responses of the GC/BP/RGO, GC/BP and GC/RGO Ca^{2+}-ISEs were recorded

and compared, as shown in Fig. 5. Testing solutions of 10^{-1} M $CaCl_2$ (labelled as phase A, the first 2 h and the last 6 h) and 10^{-1} M $MgCl_2$ (labelled as phase B, the second 2 h) were selected. Potential drifts of the GC/BP/RGO, GC/RGO, and GC/BP Ca^{2+}-ISEs were calculated to be 1.15, 1.70 and 1.52 mV h^{-1}, respectively. The GC/BP/RGO Ca^{2+}-ISE revealed a slight advantage in terms of stability compared with the other two ISEs. The hydrophobic characteristics of BP/RGO, RGO and BP effectively eliminated the water layer problem. The results corresponded well with those of similar previous studies [27, 30, 39].

3.3 Potentiometric response

The electrochemical performance of the GC/BP/RGO Ca^{2+}-ISE was systematically characterized, as shown in Fig. 6. According to the IUPAC recommendation, a quasi-Nernstian response was obtained with a potentiometric response slope of 28.3 mV/decade. The limit of detection (LOD) was found to be 7.2×10^{-6} M. The response time was determined to be 10 s. The potentiometric performance of the GC/BP/RGO Ca^{2+}-ISE was continuously measured over 10 days. The representative electrochemical characteristics are summarized in Table 1. The response slope and detection limit illustrated negligible changes over the first 24 h of detection. The response slope dropped slightly to 26.9 mV/decade on the fifth day. The detection limit increased by 18%, with the value decreasing from 7.2 to 5.9×10^{-6} M. Subsequently, the response slope slowly degraded to 25.0 mV/decade with a detection limit of 2.4×10^{-6} M on the tenth day of testing. According to the IUPAC recommendation, the lifetime of the prepared GC/BP/RGO Ca^{2+}-ISE was determined to be 10 days.

The influences of environmental parameters, including room light, UV light, NIR light, N_2, O_2, and CO_2, are shown in Fig. 7. A potential drift of 2.86 μV s^{-1} was observed when the ISE was exposed to the three tested ambient light conditions. Additionally, a potential variation of 2.48 μV s^{-1} was observed when the ISE was sequentially purged with N_2, O_2, and CO_2. The stability performance of the composite mediator layer of BP/RGO was similar to the results of previous studies on all-solid-state ISEs with the single mediator films of graphene (2.33 ± 0.28 μV s^{-1}) and three-dimensional ordered macroporous (3DOM) carbon (3.28 ± 0.42 μV s^{-1})[44-45].

The analytical characteristics of the all-solid-state Ca^{2+}-ISEs were compared among mediator films composed of graphene (GR) composites, RGO and the designed BP/RGO composite, as listed in Table 2. The proposed Ca^{2+}-ISE based on the BP/RGO composite showed a greater linear detection range than that of the other ISEs with similar robustness and lifetime performance.

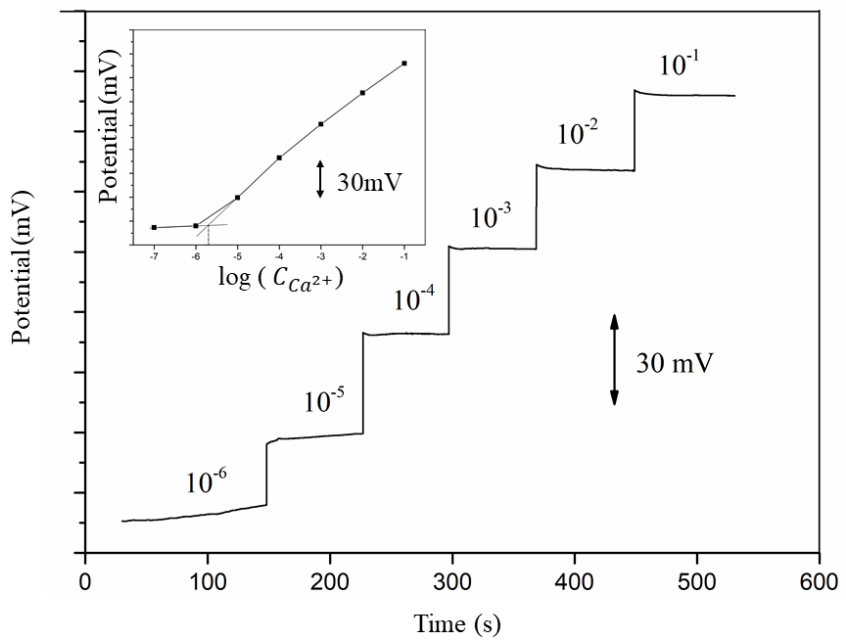

Figure 6. Potentiometric response of the GC/BP/RGO Ca^{2+}-ISE. Inset: calibration curve of the GC/BP/RGO Ca^{2+}-ISE. The measurements were recorded in $CaCl_2$ solutions ranging from 1.0×10^{-6} M to 1.0×10^{-1} M.

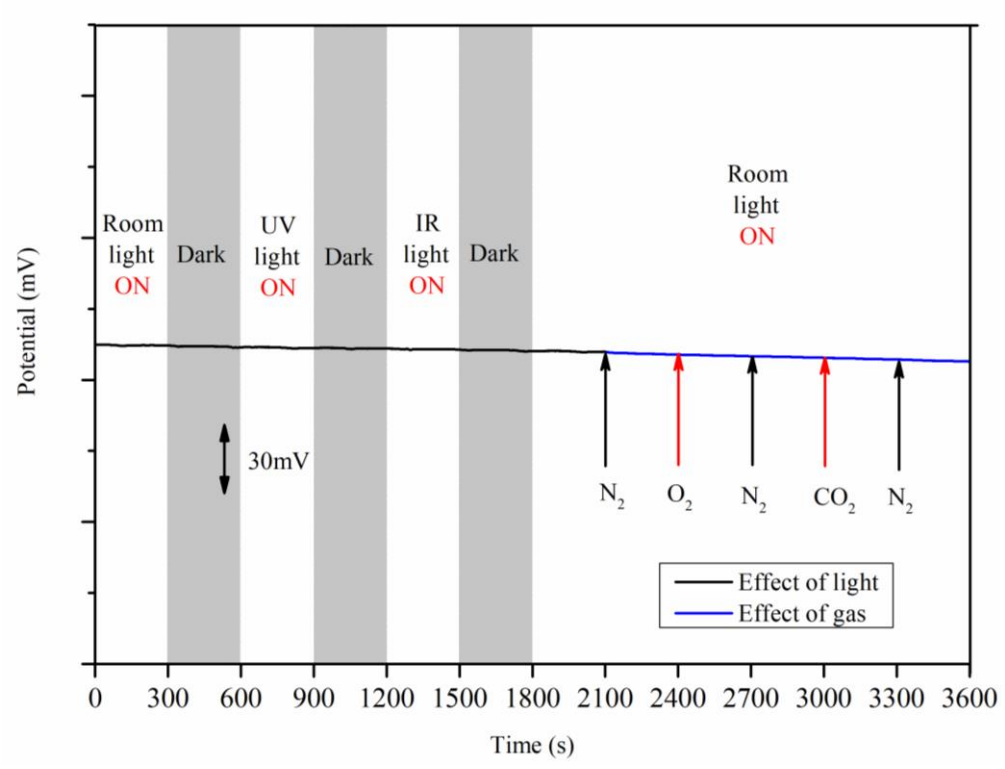

Figure 7. Potentiometric response of the GC/BP/RGO Ca^{2+}-ISE under different environmental conditions of light (black) and gas (blue) in a 10^{-1} M $CaCl_2$ solution during continuous operation for 3600 s.

Table 1. Long-term potentiometric response of the GC/BP/RGO Ca^{2+}-ISE.

Test Duration(Day)	Slope(mV/decade)	Intercept(mV)	LOD(10^{-6} M)	R^2
1	28.2	143.8	7.2	0.998
5	26.9	149.3	5.9	0.996
10	25.0	153.7	2.4	0.985

Table 2. Comparison of the analytical characteristics of GR-composite Ca-ISEs with the proposed GC/BP/RGO Ca^{2+}-ISE.

Solid contact	LOD (M)	Linear range (M)	Slope (mV/decade)	Lifetime (Day)	Reference
Fe_3O_4-RGO	4.0×10^{-7}	10^{-3}-10^{-6}	28.2	14	[16]
PANI-GR	5.0×10^{-8}	10^{-4}-3×10^{-7}	28.7	-	[39]
RGO	$10^{-5.8}$	$10^{-1.6}$-$10^{-5.6}$	29.1	14	[30]
BP-RGO	7.2×10^{-6}	10^{-1}-10^{-6}	28.3	10	our work

3.5 Hydroponic calcium determination

The feasibility of the GC/BP/RGO Ca^{2+}-ISE was evaluated for the detection of Ca^{2+} in a hydroponic lettuce nutrient solution (HLNS). Three samples were selected at different lettuce cultivation time points. The results are listed in Table 3. The Ca^{2+} contents were estimated to range from 0.44 to 1.89×10^{-4} M by the ISE, which closely matched the results obtained by a conventional flame photometer. The absolute error was approximately 0.05×10^{-4} M. The RMSE was calculated as 0.08×10^{-4} M.

Table 3. Feasibility test results for the Ca^{2+} content of hydroponic lettuce nutrient solutions as determined by the GC/BP/RGO Ca^{2+}-ISE.

Sample No.	GC/BP/RGO Ca^{2+}-ISE[a]	Flame Photometer	RMSE	Standard Addition Method		Recovery Rate
				Solution Added	Concentration Predicted [a]	
			($\times 10^{-4}$ M)			
1	0.44 ± 0.01	0.49	0.08	0.25	0.68 ± 0.06	95%
				0.50	0.88 ± 0.04	87%
2	1.01 ± 0.03	0.99		0.50	1.48 ± 0.02	93%
				1.00	1.91 ± 0.03	90%
3	1.89 ± 0.03	1.95		1.00	3.01 ± 0.10	112%
				2.00	$4.02 \pm 0.$	106%

[a] Average of three measurements.

Compared with the reported online hydroponic Ca^{2+} detection based on a commercial ISE, the detection accuracy was promisingly improved by an order of magnitude [46]. A solution-adding method was employed to calculate the detection recovery rates of the ISE according to eq. (1). Two solutions with different concentrations were selected for each of the hydroponic samples. The recovery rates varied from 87% to 112%, with an average value of 97%. The all-solid-state GC/BP/RGO Ca^{2+}-ISE exhibited satisfactory accuracy and repeatability for the detection of Ca^{2+} in a hydroponic nutrient solution.

4. CONCLUSION

In this work, an all-solid-state Ca^{2+}-ISE based on a composite mediator layer of RGO-coated BP, which was innovatively fabricated in an aqueous solution through electrochemical methods, was systematically investigated. The all-solid-state Ca^{2+}-ISE demonstrated ideal stability and sensitivity. In addition, satisfactory repeatability was obtained when applied to hydroponic Ca^{2+} detection.

ACKNOWLEDGMENTS
This research was financially supported by the National Key Research and Development Program (Grant No. 2016YFD0800900-2016YFD0800907 & 2016YFD0700300-2016YFD0700304) and Key Laboratory of Technology Integration and Application in Agricultural Internet of Things, Ministry of Agriculture, P. R. China (2016KL03).

References

1. Y. Wang, H. Xu, X. Yang, Z. Luo, J. Zhang, G. Li, *Sens. Actuators, B*, 173 (2012) 630.
2. N. Abramova, J. M. Vico, J. Soley, C. Ocaña, A. Bratov, *Anal. Chim. Acta*, 943 (2016) 50.
3. M. Lu, J. Ren, *Electrochem. Commun.*, 84 (2017) 10.
4. G. Vardar, M. Altıkatoğlu, D. Ortaç, M. Cemek, İ. Işıldak, *Biotechnol. Appl. Biochem.*, 62 (2015) 663.
5. H. J. Kim, W. K. Kim, M. Y. Roh, C. I. Kang, J. M. Park, K. A. Sudduth, *Comput. Electron. Agr.*, 93 (2013) 46.
6. J.W. Ross, *Science*, 156 (1967) 1378.
7. T. Lindfors, A. Ivaska, *Anal. Chim. Acta*, 404 (2000) 111.
8. E. Pretsch, D. Ammann, H.F. Osswald, M. Güggi, W. Simon, *Helv. Chim. Acta*, 63 (1980) 191.
9. E. Wang, W.L. Erdahl, S.A. Hamidinia, C.J. Chapman, R.W. Taylor, D.R. Pfeiffer, *Biophys. J.,* 81 (2001) 3275.
10. Z. Jingwei, Q. Yu, Z. Yunhong, *Anal. Chem.*, 82 (2010) 436.
11. T. Yin, J. Li, W. Qin, *Electroanalysis*, 29 (2017) 821.
12. J. Sutter, A. Radu, S. Peper, E. Bakker, E. Pretsch, *Anal. Chim. Acta*, 523 (2004) 53.
13. Chan, Andy D. C., and D. J. Harrison, *Anal. Chem*. 65 (1993) 32.
14. T. Yin, W. Qin, *TrAC, Trends Anal. Chem.*, 51 (2013) 79.
15. R. Hernández, J. Riu, J. Bobacka, C. Vallés, P. Jiménez, A.M. Benito, W.K. Maser, F.X. Rius, *The J. Phys. Chem. C*, 116 (2012) 22570.
16. T. Yin, X. Jiang, W. Qin, *Anal. Chim. Acta*, 989 (2017) 15.

17. V. Sorkin, Y. Cai, Z. Ong, G. Zhang, Y.W. Zhang, *Crit. Rev. Solid State Mater. Sci.*, 42 (2016) 1-82.
18. H. Liu, K. Hu, D. Yan, R. Chen, Y. Zou, H. Liu, S. Wang, *Adv. Mater.,* (2018) 1800295.
19. R.A. Doganov, E.C. O'Farrell, S.P. Koenig, Y. Yeo, A. Ziletti, A. Carvalho, D.K. Campbell, D.F. Coker, K. Watanabe, T. Taniguchi, A.H. Castro Neto, B. Ozyilmaz, *Nat. Commun.*, 6 (2015) 6647.
20. J. D. Wood, S.A. Wells, D. Jariwala, K. S. Chen, E. K. Cho, V. K. Sangwan, X. Liu, L. J. Lauhon, T. J. Marks, M. C. Hersam, *Nano Lett.*, 14 (2014) 6964.
21. R. A. Doganov, E. C.T. O'Farrell, S. P. Koenig, Y. Yeo, A. Ziletti, A. Carvalho, D. K. Campbell, D. F. Coker, K. Watanabe, T. Taniguchi, A. H. C. Neto, B. Özyilmaz, *arXiv* (2014) arXiv:1412.1274.
22. B. Wan, B. Yang, Y. Wang, J. Zhang, Z. Zeng, Z. Liu, W. Wang, *Nanotechnology*, 26 (2015) 435702.
23. J. Kim, S.K. Baek, K.S. Kim, Y.J. Chang, E.J. Choi, *Curr. Appl. Phys.*, 16 (2016) 165.
24. X. Li, W Cai, J. An, S. Kim, J. Nah, D. Yang, R. Piner, A. Velamakanni, I. Jung, E. Tutuc, S. K. Banerjee, L. Colombo, R. S. Ruoff, *Science*, 324 (2009) 1312.
25. Y. Huang, J. Qiao, K. He, S. Bliznakov, E. Sutter, X. Chen, D. Luo, F. Meng, D. Su, J. Decker,W. Ji, R. S, Ruoff, P. Sutter, *Chem. Mater.*, 28 (2016) 8330.
26. X. Li, X. Niu, W. Zhao, W. Chen, C. Yin, Y. Men, G. Li, W. Sun, *Electrochem. Commun.*, 86 (2018) 68.
27. L. Kou, M. Fu, R. Liang, *RSC Adv.*, 7 (2017) 43905.
28. P. Yasaei, B. Kumar, T. Foroozan, C. Wang, M. Asadi, D. Tuschel, J. E. Indacochea, R. F. Klie, A. Salehi-Khojin, *Adv. Mater.*, 27 (2015) 1887.
29. D. Hanlon, C. Backes, E. Doherty, C. S. Cucinotta, N. C. Berner, C. Boland, K. Lee, A. Harvey, P. Lynch, Z. Gholamvand, S. Zhang, K. Wang, G. Moynihan, A. Pokle, Q. M. Ramasse, N. McEvoy, W. J. Blau, J. Wang, G. Abellan, F. Hauke, A. Hirsch, S. Sanvito, D. D. O'Regan, G. S. Duesberg, V. Nicolosi, J. N. Coleman, *Nat. Commun.*, 6 (2015) 8563.
30. J. Ping, Y. Wang, Y. Ying, J. Wu, *Anal. Chem.*, 84 (2012) 3473.
31. M. Zhou, Y. Wang, Y. Zhai, J. Zhai, W. Ren, F. Wang, S. Dong, *Chem. Eur. J.*, 15 (2009) 6116.
32. J. Ping, Y. Wang, K. Fan, J. Wu, Y. Ying, *Biosens. Bioelectron.*, 28 (2011) 204-209.
33. H. Liu, Y. Zou, L. Tao, Z. Ma, D. Liu, P. Zhou, H. Liu, S. Wang, *Small*, 13 (2017) 1700758.
34. D. Long, W. Li, L. Ling, J. Miyawaki, I. Mochida, S. H. Yoon, *Langmuir*, 26 (2010) 16096.
35. J. Bobacka, *Anal. Chem.*, 71 (1999) 4932.
36. E. Lindner, Y. Umezawa, *Pure Appl. Chem*., 80 (2008) 85.
37. Resh, M. Howard, Hydroponic Food Production, *Crc Press*, (2012) California, America.
38. L. Zhang, M. Zhang, H. Ren, P. Pu, P. Kong, H. Zhao, *Comput. Electron. Agr.*, 112 (2015) 83.
39. Z. A. Boeva, T. Lindfors, *Sens. Actuators, B*, 224 (2016) 624.
40. H. Rafael, R. Jordi, R. F Xavier, *Analyst*, 135 (2010) 1979-1985.
41. P. Li, D. Zhang, J. Liu, H. Chang, Y. Sun, N. Yin, *ACS Appl. Mater. Interfaces*, 7 (2015) 24396.
42. Y. Zhu, S. Murali, W. Cai, X. Li, J. W. Suk, J. R. Potts, R. S. Ruoff, *Adv. Mater.*, 22 (2010) 3906.
43. T. Lindfors, F. Sundfors, L. Höfler, R. E. Gyurcsányi, *Electroanalysis*, 21 (2010) 1914-1922.
44. F. Li, J. Ye, M. Zhou, S. Gan, Q. Zhang, D. Han, L. Niu, *Analyst*, 137 (2012) 618-623.
45. C. Z. Lai, M. A. Fierke, A. Stein, P. Bühlmann, *Anal. Chem.*, 79 (2007) 4621.
46. W.J. Cho, H.J. Kim, D.H. Jung, D.W. Kim, T.I. Ahn, J.E. Son, *Comput. Electron. Agr*., 146 (2018) 51.